MOMENT MODEL OF NONUNIFORM CHANNEL-BEND FLOW. II: ERODIBLE BEDS

By Keh-Chia Yeh,[1] Associate Member, ASCE, and John F. Kennedy,[2] Member, ASCE

ABSTRACT: The hybrid integral-differential moment and momentum model of fixed-boundary channel-bend flows developed in the companion paper is extended to erodible-bed flows. The θ unit sediment discharge is formulated as a power of local depth-averaged θ velocity; and the *r* unit sediment discharge as proportional to the ratio of the excess of the *r* bed shear stress, over the radial component of the submerged weight of the sediment bed layer, to the θ bed shear stress. Bed topography is computed from two-dimensional (2D) sediment continuity. The resulting two coupled sets of simultaneous equations are solved numerically. The model yields accurate predictions of the velocities (primary and secondary), and 2D bed topography. The average radial bed slope, primary velocity-profile exponent, and secondary rotational and translational velocities exhibit much larger variations along the channel than in fixed-boundary bends. The increased variation and oscillatory behavior of these quantities are elucidated from moment-of-momentum conservation and interaction of bed topography and flow.

INTRODUCTION

An extension of the analytical model of fixed-boundary nonuniform bend flow described in part I (Yeh and Kennedy 1993) to flows in erodible-bed channel bends is developed herein. The channel plan and much of the notation are defined in Fig. 1 of part I. The development parallels that of Struiksma et al. (1985), Odgaard (1986), Nelson (1988), and Shimizu et al. (1990). Special features of the models are summarized by Parker and Johannesson (1989).

PHYSICAL DESCRIPTION

Four principal aspects of erodible-bed channel-bend (river) flow differentiate it from flow in straight erodible-bed channels: sediment discharge across the channel; warped bed topography; skewed distribution of the primary flow; and radial-plane rotational and translational flows (the so-called secondary flows). The bed deformation results principally from two mechanisms, as follows.

The first is the radial bed shear stress produced by the secondary rotational and translational velocities, u_s and u_t. The secondary rotational velocity is always directed radially inward near the bed, and is usually somewhat greater than u_t (which, recall from part I, changes direction along the bend). Consequently, the radial shear stress acting on the bed, τ_{0r}, is directed inward and transports sediment in this direction. This tendency is resisted by the

[1]Assoc. Prof., Dept. of Civ. Engrg., Nat. Chiao Tung Univ., Hsinchu, Taiwan 30050, Republic of China.

[2]Deceased; formerly Hunter Rouse Prof. of Hydr. and Dir., Inst. of Hydr. Res., Univ. of Iowa, Iowa City, IA 52242-1585.

Note. Discussion open until December 1, 1993. Separate discussions should be submitted for the individual papers in this symposium. To extend the closing date one month, a written request must be filed with the ASCE Manager of Journals. The manuscript for this paper was submitted for review and possible publication on August 21, 1991. This paper is part of the ***Journal of Hydraulic Engineering***, Vol. 119, No. 7, July, 1993. ©ASCE, ISSN 0733-9429/93/0007-0796/$1.00 + $.15 per page. Paper No. 2530.

radial slope of the bed, S_T, which produces a downslope outward force (in the radial vertical plane) on the moving layer of bed particles (the bed layer). The radial near-bed velocity and resultant radial bed shear transport sediment toward the inner bank until the areal distribution of S_T is such that radial-force equilibrium, between shear and gravity forces, of the bed layer is attained (with allowance made for the second mechanism, discussed in the next paragraph) at every point on the bed.

The second important effect of sediment transport arises from the redistribution of the flow (unit discharge) across the channel. The unit sediment discharge generally increases with increasing unit water discharge, and therefore the continuous radial redistributions along the channel of V (= local depth-averaged velocity) and d are accompanied by a corresponding redistribution of unit sediment discharge. The radial sediment transport produced by u_s and u_t generally is inadequate to satisfy the two-dimensional (2D) sediment-continuity equation; indeed, along some reaches (e.g., between sections 1 and 2 in Fig. 1 of part I) the near-bed radial velocity is in the wrong direction to do so. Consequently, the radial bed slope is increased or decreased by local deposition or scour and thereby modulates the radial sediment transport as required to satisfy sediment continuity. Due to the overshoot of the secondary rotational flow, discussed in part I, oversteepening of the radial bed slope and subsequent downstream spatial damped oscillation of the radial bed slope toward equilibrium can occur along the upstream part of river bends.

The bed deformation also affects M_r and M_θ [= θ fluxes of radial and streamwise moment of momentum (MOM)] in very important ways, which can be illustrated by examining the effect of radial bed slope on them, as was done by Yeh (1990). Fig. 1 shows the effect of the bed slope $\tilde{S}_T[=\bar{S}_T b/(2d_0)][\bar{S}_T(\theta)$ = average radial bed slope; d_0 = mean flow depth; and b = channel width] of a vertical-wall channel section on the normalized θ MOM (computed about the centroid of the undeformed, rectangular section). Note that M_θ can even become negative as $\tilde{S}_T$ increases.

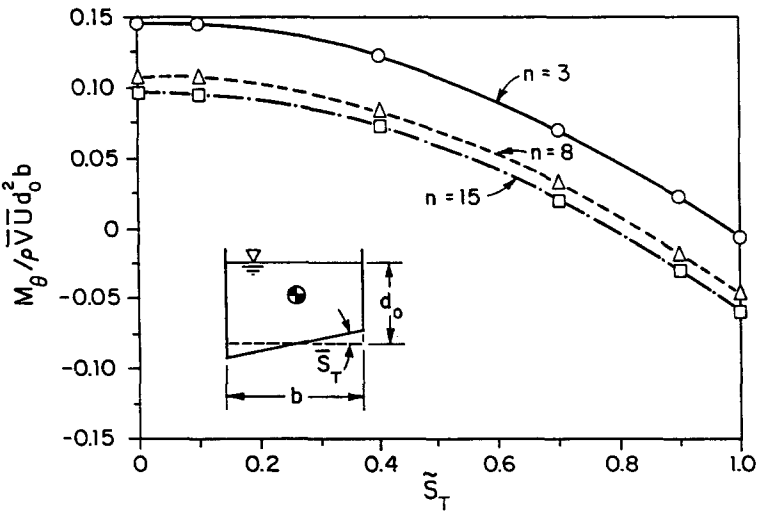

FIG. 1. Variation of $M_\theta/\rho\bar{V}\bar{U}d_0^2b$ with $\tilde{S}_T$ for Trapezoidal Section ($\bar{U}_t/\bar{U}$ = 1.0; γ = 0.5; M_θ is Computed about Centroid of Original Rectangular Section

As can be seen from the MOM balances portrayed in Fig. 2 of part I, M_r decreases along the upstream part of the bend (due to the negative influx of M_θ, and to the increase of $\tilde{S}_T$), and hence $n(\theta)$ (= inverse exponent in power-law velocity profile) increases. However, as M_θ decreases and possibly changes sign with increasing $\tilde{S}_T$ (see Fig. 1), the negative influx of M_θ into M_r decreases, and thus M_r increases and n decreases. Consequently, n may overshoot its equilibrium curved-channel value and then decrease. The changes in n affect the centrifugal moment, and thus also the strength of the secondary rotational velocity and $\tilde{S}_T$, which in turn modulate n. Additionally, the radial steepening of the bed as $\tilde{S}_T$ tends toward its maximum increases the radially outward secondary translational velocity, u_t, and redistributes the unit water and sediment discharges across the channel, both of which affect $\tilde{S}_T$. Consequently, the radial bed slope, secondary rotational flow, and n undergo damped spatial oscillation along the transition reach of the bend; $\bar{U}_t$ (= section-averaged secondary translational velocity) also is spatially oscillatory, due to the oscillation of $\tilde{S}_T$. The maxima of $\tilde{S}_T$ lag those of n. As $\tilde{S}_T$ retreats from its maximum toward its equilibrium value, the magnitudes of M_r and M_θ first decrease and then oscillate along the channel (due to the variation of M_θ resulting from the oscillation of $\tilde{S}_T$), and n, after initially increasing, oscillates toward equilibrium.

Mathematical Formulation

Integrated MOM Equations

The r- and θ-direction MOM equations again are obtained from the lettered terms plus the term $\rho u \partial u/\partial r$ (which cannot be neglected in the case of deformed beds) in (1)–(3) of part I. Note that the strong warping of the bed along the bend significantly increases the r and θ gradients of the velocities. Consequently, u is taken to be distributed as function of r and θ

$$U(r, \theta) = \delta \frac{r_c}{r} \frac{d}{d_0} \frac{V}{\bar{V}} \bar{U} \quad \ldots\ldots (1)$$

where δ = correction factor given by

$$\delta = \frac{\int_{r_o}^{r_i} U \, dr}{\int_{r_o}^{r_i} \frac{r_c}{r} \frac{d}{d_0} \frac{V}{\bar{V}} \bar{U} \, dr} \quad \ldots\ldots (2)$$

and r_c = channel-centerline radius. Eq. (1) is suggested by the analytical results of several investigators (Falcon and Kennedy 1983). In keeping with (1), τ_{0r} is expressed as

$$\tau_{0r} = -\alpha \tau_{0\theta} \frac{1}{\bar{V}} \left(\delta \frac{r_c}{r} \frac{d}{d_0} \frac{V}{\bar{V}} \bar{U} + U_t \right) \quad \ldots\ldots (3)$$

Note that r- and θ-dependent velocities, $V(r, \theta)$, $U(r, \theta)$, and $U_t(r, \theta)$ are used in the velocity and shear-stress relations [(14)–(16), (19)–(21), and (23), in part I; $V(r, \theta)$, $U_t(r, \theta)$, and $d(r, \theta)$ are obtained from differential depth-integrated momentum and continuity equations, as described in the next section.

Because the bed topography now is a dependent variable, the integrations of the MOM equations must be accomplished numerically. Proceeding as

for the fixed-bed case, adopting $\xi = 0.5$ [see (16) in part I], and taking moments about the centroid of the original undeformed cross section yields the following θ and r MOM equations:

$$\frac{1}{r}\frac{d}{d\theta}\left(\frac{\bar{U}}{\bar{V}}\right)\int_{r_i}^{r_o}\frac{V}{\bar{V}}\left(\frac{d}{d_0}\right)^2 GH\,dr + \int_{r_i}^{r_o}\frac{V}{\bar{V}}\left(\frac{d}{d_0}\right)^2\frac{\bar{U}}{\bar{V}}\frac{1}{r}\frac{\partial}{\partial\theta}(GH)\,dr - 2$$

$$\cdot\int_{r_i}^{r_o}\frac{V}{\bar{V}}\frac{d}{d_0}\frac{1}{r}\frac{\partial}{\partial\theta}\left(\frac{d}{d_0}\right)\left(G\frac{\bar{U}}{\bar{V}}\right)\left[-\frac{n(n+1)}{(2n+1)(3n+1)} + \frac{n+1}{2(2n+1)}\frac{d_0}{d}\right]dr$$

$$+\int_{r_i}^{r_o}\frac{V}{\bar{V}}\left(\frac{d}{d_0}\right)^2\frac{1}{r}\frac{\partial}{\partial\theta}\left(\frac{U_t}{\bar{V}}\right)I\,dr - \int_{r_i}^{r_o}\frac{1}{r}\left(\frac{V}{\bar{V}}\right)^2\left(\frac{d}{d_0}\right)^2\left[\frac{1}{2(n+2)}\right.$$

$$\left.+\frac{1}{2n(n+2)}\frac{d_0}{d}\right]dr + 2\int_{r_i}^{r_o}\gamma\delta\left(\frac{\bar{U}}{\bar{V}}\right)^2\frac{1}{d_0}\left(\frac{d}{d_0}\right)^2\frac{d_c}{b}\frac{r-r_c}{b}\frac{r_c}{r}\frac{V}{\bar{V}}$$

$$\cdot\left(1-\frac{d_0}{d}\right)dr + 2\int_{r_i}^{r_o}\gamma\frac{d_c}{b^2}\frac{d}{d_0^2}\frac{\bar{U}}{\bar{V}}\frac{U_t}{\bar{V}}(r-r_c)\,dr + 2\int_{r_i}^{r_o}\gamma\frac{V}{\bar{V}}\frac{d}{d_0}$$

$$\cdot\left[\frac{d_c}{b^2 d_0}\frac{1}{r}\frac{\partial}{\partial\theta}\left(\frac{\bar{U}}{\bar{V}}\right) + \frac{1}{b^2}\frac{\bar{U}}{\bar{V}}\frac{1}{r}\frac{\partial}{\partial\theta}\left(\frac{d_c}{d_0}\right)\right](r-r_c)^2\,dr = \frac{1}{8}\alpha f\int_{r_i}^{r_o}\frac{1}{d_0}\frac{V}{\bar{V}}$$

$$\cdot\left(-G\frac{\bar{U}}{\bar{V}} + \frac{U_t}{\bar{V}}\right)\left(\frac{d}{d_0}-\frac{1}{2}\right)dr - \frac{1}{16}\beta f\left[\frac{1}{r_c}\frac{d_c}{d_0}\frac{\bar{U}}{\bar{V}}\left(\frac{d_{ou}}{d_0}r_o - \frac{d_{in}}{d_0}r_i\right)\right] \quad \ldots\ldots (4)$$

and

$$\int_{r_i}^{r_o}\left(\frac{d}{d_0}\right)^2\frac{\partial}{\partial r}\left(\frac{V}{\bar{V}}\right)\left(GH\frac{\bar{U}}{\bar{V}} + I\frac{U_t}{\bar{V}}\right)dr - \int_{r_i}^{r_o}\frac{1}{n}\frac{V}{\bar{V}}\frac{d}{d_0}\frac{\partial}{\partial r}\left(\frac{d}{d_0}\right)\left(GH\frac{\bar{U}}{\bar{V}}\right.$$

$$\left.+ I\frac{U_t}{\bar{V}}\right)dr - \int_{r_i}^{r_o}\left(\frac{V}{\bar{V}}\right)^2\left(\frac{d}{d_0}\right)^2\frac{1}{r}\frac{dn}{d\theta}\frac{n+1}{n^3}J\,dr + \frac{1}{2}\int_{r_i}^{r_o}\left(\frac{d}{d_0}\right)^2\frac{1}{r}\frac{\partial}{\partial\theta}\left(\frac{V}{\bar{V}}\right)^2$$

$$\cdot\left(\frac{n+1}{n}\right)^2 J\,dr - \int_{r_i}^{r_o}\left(\frac{V}{\bar{V}}\right)^2\frac{d}{d_0}\frac{1}{r}\frac{\partial}{\partial\theta}\left(\frac{d}{d_0}\right)\frac{(n+1)^2}{n^3}J\,dr + \int_{r_i}^{r_o}\left(\frac{V}{\bar{V}}\right)^2$$

$$\cdot\left(\frac{d}{d_0}\right)^2\ln\left(\frac{d}{d_0}\right)\frac{1}{r}\frac{dn}{d\theta}\frac{(n+1)^2}{n^4}J\,dr + \int_{r_i}^{r_o}\frac{1}{r}\frac{V}{\bar{V}}\left(\frac{d}{d_0}\right)^2\left(GH\frac{\bar{U}}{\bar{V}} + I\frac{U_t}{\bar{V}}\right)dr$$

$$+ 2\int_{r_i}^{r_o}\gamma\frac{\bar{U}}{\bar{V}}\frac{d_c}{b}\frac{r-r_c}{b}\frac{V}{\bar{V}}\frac{d}{d_0^2}\left(1-\frac{1}{2}\frac{n+1}{n}\frac{d_0}{d}\right)dr = gS_0\int_{r_i}^{r_o}\left(\frac{d}{d_0}\right)^2\left(\frac{1}{\bar{V}}\right)^2$$

$$\cdot\left(-\frac{1}{2}+\frac{1}{2}\frac{d_0}{d}\right)dr + \frac{1}{8}f\int_{r_i}^{r_o}\left(\frac{V}{\bar{V}}\right)^2\frac{1}{d_0}\left(\frac{d}{d_0}-\frac{1}{2}\right)dr - \frac{1}{8}f$$

$$\cdot\int_{r_i}^{r_o}\left(\frac{V}{\bar{V}}\right)^2\frac{d}{d_0^2}\frac{n_e^4}{n_e+1}C\,dr \quad \ldots\ldots (5)$$

where d_{in}, d_{ou} = flow depths at the inner and the outer wall, respectively; S_0 = channel streamwise bed slope; C is defined in (28) in part I; and

$$G = \delta \frac{r_c}{r} \frac{d}{d_0} \frac{V}{\bar{V}} \quad \text{..... (6)}$$

$$H = \frac{n(n-1)}{(2n+1)(3n+1)} + \frac{1}{2(2n+1)} \frac{d_0}{d} \quad \text{..... (7)}$$

$$I = -\frac{n}{2n+1} + \frac{1}{2} \frac{d_0}{d} \quad \text{..... (8)}$$

and

$$J = \frac{-n^2}{2(n+1)(n+2)} + \frac{n}{2(n+2)} \frac{d_0}{d} \quad \text{..... (9)}$$

Because moments are not computed about the centroid of the deformed cross section, it is necessary to retain the pressure term $\{(1/r)[\partial(r\sigma_{rr})/\partial r]$ in (1), in part I} in the integration. Eqs. (4) and (5) are a system of first-order nonlinear ordinary differential equations for $\bar{U}(\theta)$ and $n(\theta)$.

Depth-Integrated Momentum and Continuity Equations

The depth-integrated θ-momentum equation and continuity equations are used in the calculation of $V(r, \theta)$ and $U_t(r, \theta)$ for computed values of $\bar{U}$, n, and d. Depth integration of (31) in part I, after substituting the appropriate relations for the velocities and stresses yields

$$\frac{(n+1)^2}{n(n+2)} \frac{d}{r} \frac{\partial}{\partial \theta} \left(\frac{V}{\bar{V}}\right)^2 + \left[\frac{1}{8} f + \frac{(n+1)^2}{n(n+2)} \frac{1}{r} \frac{\partial d}{\partial \theta} - \frac{2(n+1)}{n^2(n+2)^2} \frac{d}{r} \left(\frac{\partial n}{\partial \theta}\right)\right]$$

$$\cdot \left(\frac{V}{\bar{V}}\right)^2 = \frac{1}{\bar{V}^2} g S_0 d - \frac{r - r_c}{r} \frac{\partial}{\partial \theta} \left(\frac{d}{r_c}\right) - \frac{\partial}{\partial r} \left(\frac{V}{\bar{V}} dF\right) - 2 \frac{d}{r} \frac{V}{\bar{V}} F \quad \text{..... (10)}$$

$$F = \frac{1}{2n+1} \delta \frac{r_c}{r} \frac{d}{d_0} \frac{V}{\bar{V}} \frac{\bar{U}}{\bar{V}} + \frac{U_t}{\bar{V}} \quad \text{..... (11)}$$

The depth-integrated water-continuity relation is

$$\frac{1}{r} \frac{\partial}{\partial r} (r U_t) = -\frac{1}{r} \frac{\partial V}{\partial \theta} \quad \text{..... (12)}$$

Bed-Slope Relation

Ikeda and Nishimura (1986) found that the influence of suspended-load discharge on the bed topography of river bends is relatively minor and generally can be neglected. Therefore, only the bed-load discharge is considered here. The bed-load transport in the r-direction is controlled principally by radial bed-shear and gravity forces. It will be assumed that the lateral unit sediment discharge is proportional to the difference between the shear and the gravity forces, exerted on the moving bed-surface layer; i.e.

$$\frac{q_r}{q_\theta} = \left(\frac{\text{excess radial component of submerged weight of bed-layer}}{\text{unit area}}\right)\eta$$

$$= \frac{(S_T - S_{T0})y_b(1 - p_s)\rho' g}{\tau_{0\theta}}\eta \quad \ldots\ldots (13)$$

in which q_r, q_θ = radial and streamwise unit sediment discharge; $S_T(r, \theta)$ = local radial bed slope; S_{T0} = slope required to overcome the radial bed shear stress, i.e., to produce radial-plane force equilibrium of the bed layer; y_b = bed-layer thickness; p_s = bed-material porosity; $\rho' = \rho_s - \rho$; $\tau_{0\theta}$ = streamwise bed shear stress; and η = a constant. When the local radial bed slope S_T equals the equilibrium bed slope, S_{T0}, the lateral sediment transport is zero and it then follows from (13) that:

$$S_{T0} = -\frac{\tau_{0r}}{y_b(1 - p_s)\rho' g} \quad \ldots\ldots (14)$$

Note that the equilibrium bed slope S_{T0} can be expressed in terms of primary flow variables by substituting (3) for τ_{0r} and (15) for y_b, in which the shear velocities can again be expressed in terms of primary velocity and sediment properties.

According to Karim and Kennedy's (1981) concept, the bed-layer thickness, y_b, is given by

$$y_b = C_b D_{50}\frac{u_*}{u_{*c}} \quad \ldots\ldots (15)$$

where C_b = correction factor incorporated here to extend the transport relation to other than the primary-flow direction for which it was derived; D_{50} = median bed-material size; and u_{*c} = critical shear velocity for initiation of bed-material motion, as obtained from Shields' diagram.

The radial bed slope S_T is obtained from the 2D equation of sediment continuity

$$\frac{1}{r}\frac{\partial q_\theta}{\partial \theta} = -\frac{1}{r}(rq_r) \quad \ldots\ldots (16)$$

Integration of (16) with respect to r and normalization by $\bar{q}_\theta$ (= q_θ corresponding to the section-averaged velocity $\bar{V}$) yields

$$\frac{q_r}{\bar{q}_\theta} = -\frac{1}{r}\int_{r_i}^{r} r\frac{\partial}{\partial s}\left(\frac{q_\theta}{\bar{q}_\theta}\right)dr \quad \ldots\ldots (17)$$

A power-law sediment-discharge relation in the streamwise direction is adopted

$$\frac{q_\theta}{\bar{q}_\theta} = \left(\frac{V}{\bar{V}}\right)^K \quad \ldots\ldots (18)$$

where the exponent K = a function of the flow and sediment characteristics. In straight alluvial channels, K is generally between two and four (Simons and Sentürk 1977). Substitution of (3), (14), (15), (17), and (18) into (13) and letting $u_* = V(f/8)^{1/2}$; $u_{*c} = (g\rho'/\rho D_{50}\varphi)^{1/2}$ in which φ = dimensionless shear stress obtained from Shields' diagram; leads to

$$S_T(r, \theta) = \frac{1}{\eta}\left(\frac{V}{\bar{V}}\right)^{-K}\left[-\frac{1}{r}\int_{r_i}^{r} r\frac{\partial}{\partial s}\left(\frac{V}{\bar{V}}\right)^{K} dr\right]\frac{\sqrt{f\varphi}V}{C_b\sqrt{8g\frac{\rho'}{\rho}D_{50}(1-p_s)}}$$

$$-\frac{\sqrt{f\varphi}\alpha(-U+U_t)}{C_b\sqrt{8g\frac{\rho'}{\rho}D_{50}(1-p_s)}} \quad \ldots\ldots (19)$$

Because of the small radial water-surface slope, the local depth can be well approximated by integration of

$$\frac{\partial d}{\partial r} = S_T \quad \ldots\ldots (20)$$

Eqs. (10), (12), and (20) with S_T given by (19) are a system of strongly coupled nonlinear partial differential equations for the unknowns $V(r, \theta)$, $U_t(r, \theta)$, and $d(r, \theta)$ and are solved numerically.

Numerical Solution

The numerical scheme used in the solution of the MOM equations [(4) and (5)] for $\bar{U}(\theta)$ and $n(\theta)$, the θ momentum and continuity equations [(10) and (12)] for $V(r, \theta)$ and $U_t(r, \theta)$, and the bed-topography relations [(20)] for $d(r, \theta)$ is the same as that for the fixed-bed case (part I), except for the following.

It is observed experimentally that the flow area remains almost constant along a channel bend. Accordingly, the depth, $d(r, \theta)$, obtained from (20) at each computational grid point was linearly adjusted in proportion to its relative magnitude to yield constant flow area along the bend. Alternatively, the adjustments could have been made so as to yield constant discharge.

During the iterations for solving $d(r, \theta)$, (18) does not necessarily yield constant sediment discharge along the bend. Therefore, deviations of the computed sediment discharge from the inflow value were prorated among the computation points across each section in proportion to the local computed q_θ, to assure constancy of sediment discharge.

Because the variations of local S_T between sequential computations must be relatively small, else computational instability may occur, the following relaxation relation was adopted:

$$(S_T)_{\text{new}} = \omega(S_T)_{\text{new}} + (1-\omega)(S_T)_{\text{old}} \quad \ldots\ldots (21)$$

where ω = relaxation parameter; $(S_T)_{\text{new}}$ = updated S_T; and $(S_T)_{\text{old}}$ = previous S_T. It was found that $\omega = 0.2$ yielded stability for all flows computed.

Verification and Analysis

The values of the parameters related to velocities and stresses {$\xi = 0.5$ [(16) in part I]; $\gamma = 0.3$ [(17) in part I and (4) and (5) in part II]; $\alpha = 6$ [(20) in part I and (3) in part II]; and $\beta = 1$ [(21) in part I and (4) in part II]} determined for the fixed-bed case were found to be valid also for erodible-bed bends. The exponent, K, in the power-law streamwise sediment-discharge relation [(18)] was taken to be $K = 3$. The parameters, η [(13)], and C_b [(15)], were evaluated by calibrating the model against two of Struiks-

TABLE 1. Flows Used in Evaluation of Constants and Verification of Erodible-Bed Analytical Model

Author(s) (1)	Bend Radii r_o (m) (2)	Bend Radii r_i (m) (3)	Bend Radii r_c (m) (4)	Bend Radii θ_0 (degrees) (5)	Width b (m) (6)	b/r_c (7)	Discharge (l/s) (8)	Depth d_0 (m) (9)	Mean velocity $\bar{V}$ (m/s) (10)	Water-surface slope S_w (10^{-3}) (11)	Friction factor f (12)	Mean sediment size D_{50} (mm) (13)
Struiksma (1983)												
T1	12.75	11.25	12	140	1.5	0.125	47.0	0.080	0.39	2.36	0.0973	0.45
T2	12.75	11.25	12	140	1.5	0.125	61.0	0.100	0.41	2.03	0.0946	0.45
T3	12.75	11.25	12	140	1.5	0.125	74.0	0.091	0.54	4.19	0.1023	0.45
Olesen (1985)												
T5	12.75	10.25	11.75	140	2.0	0.17	125.0	0.135	0.46	1.49	0.0734	0.84
Odgaard and Bergs (1988)	14.23	11.99	13.11	180	2.24	0.17	153.0	0.165	0.45	1.16	0.074	0.30

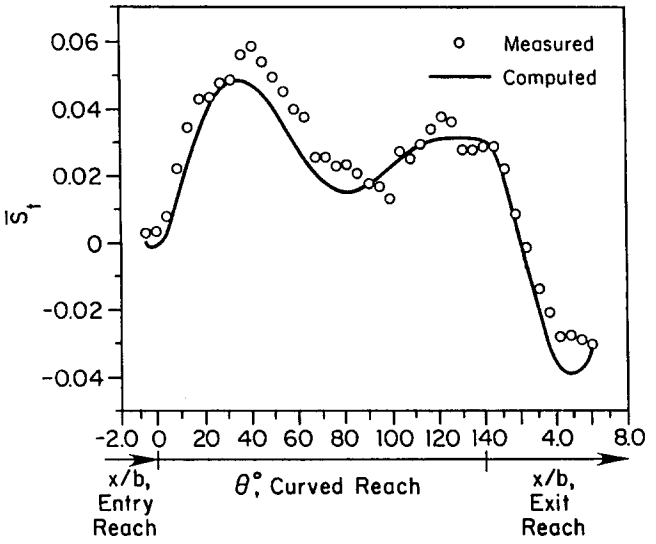

FIG. 2. Measured and Computed $\bar{S}_T$ for Struiksma's (1983) Run T1

ma's (1983) experiments, runs T1 and T2. These flows and those utilized in verifying the model are described in Table 1. Optimal conformity of analytical and experimental results, as judged visually from comparative graphs, was obtained for $\eta = 0.2$, and $C_b = 0.75$. A porosity of $p_s = 0.35$ was used for all erodible-bed computations.

Only the results for run T1 are included here. Others are reported by Yeh (1990). Fig. 2 shows the streamwise variations of radial average bed slope, $\bar{S}_T(\theta)$, which provides a rough, overall description of the channel-bed-topography variation along the bend. The overshoot of the radial bed slope (the oversteepening of the bed) and its subsequent damped oscillation are well reproduced. Fig. 3 shows the streamwise variations of flow depth near the walls for this flow, and the computed streamwise variations of $V/\bar{V}$ near the walls are presented in Fig. 4. A comparison of Figs. 2 and 4 shows that the maximum (minimum) value of $V/\bar{V}$ near the outer (inner) wall occurs downstream from the maximum oversteepening of the bed. The accompanying oscillation of n can be seen in Fig. 5, and the damped oscillations of $\bar{U}/\bar{V}$ and $\bar{U}_t/\bar{V}$ are apparent in Fig. 6. Comparisons of computed and measured lateral distributions of d/d_0 at representative sections are plotted in Fig. 7, and Fig. 8 shows comparisons of the lateral distributions of $V/\bar{V}$. The agreement between computed and measured values seen in Figs. 2, 3, 7, and 8 is, in general, very good. It should be noted that Struiksma (1983) reported that the velocity data for his experiments are not very accurate due to the sparse measurements.

It is of interest to compare the relative magnitudes of the individual terms of the θ-direction momentum equation [(31) in part I]. Recall that this equation incorporates the continuity equation and reads

$$\rho\left[\frac{\partial}{\partial r}(uv) + \frac{1}{r}\frac{\partial v^2}{\partial \theta} + \frac{2uv}{r} + \frac{\partial}{\partial z}(vw)\right] = \rho g_\theta + \frac{1}{r}\frac{\partial \sigma_{\theta\theta}}{\partial \theta} + \frac{\partial \tau_{\theta z}}{\partial z} \quad \ldots\ldots (22)$$

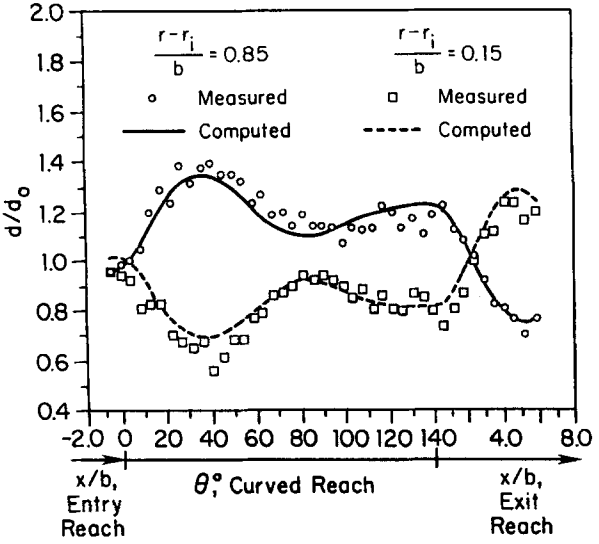

FIG. 3. Measured and Computed Depths at 0.85b and 0.15b from Convex Wall for Struiksma's (1983) Run T1

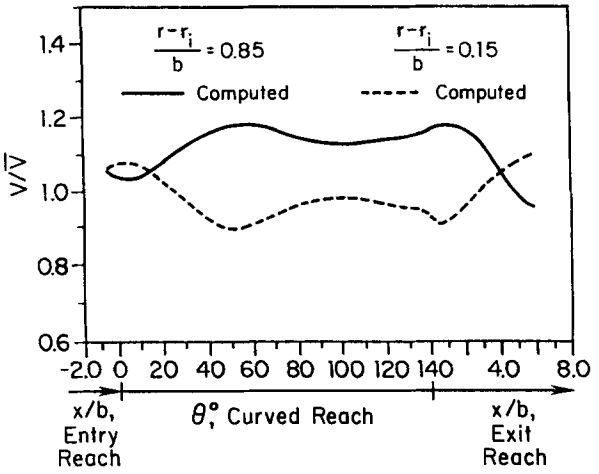

FIG. 4. Computed $V/\bar{V}$ at 0.85b and 0.15b from Convex Wall for Struiksma's (1983) Run T1

Depth-integration of (22) after applying the kinematic boundary conditions given by (33) and (34) in part I leads to

$$\rho\left[\frac{\partial}{\partial r}\int_{z_b}^{z_w} uv\,dz + \frac{1}{r}\frac{\partial}{\partial \theta}\int_{z_b}^{z_w} v^2\,dz + 2\int_{z_b}^{z_w}\frac{uv}{r}\,dz\right] = \rho g S_0 d$$

1 2 3 4

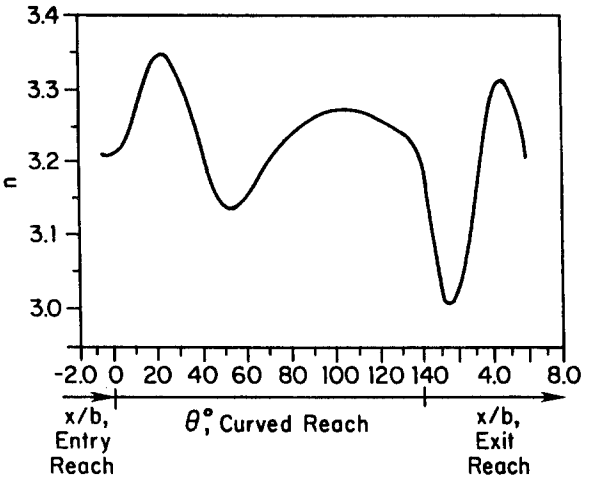

FIG. 5. Computed Streamwise Variation of n for Struiksma's (1983) Run T1

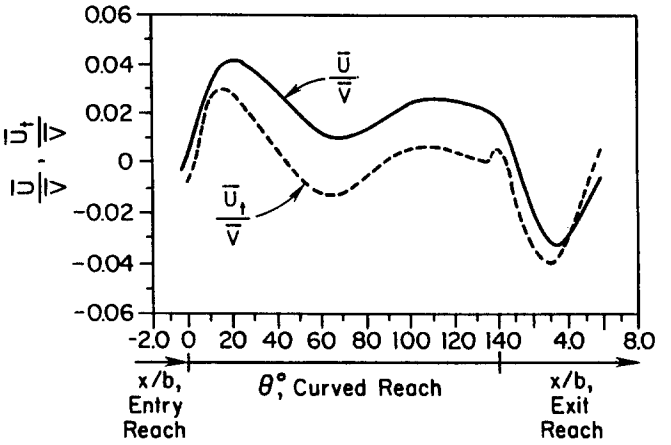

FIG. 6. Computed $\bar{U}/\bar{V}$ and $\bar{U}_t/\bar{V}$ for Struiksma's (1983) Run T1

$$+ \int_{z_b}^{z_w} \frac{1}{r} \frac{\partial \sigma_{\theta\theta}}{\partial \theta}\, dz - \tau_{0\theta} \qquad \text{(23)}$$

(5) (6)

Fig. 9 shows the magnitude of each term (except term 3) in (23) for Struiksma's (1983) run T1. Due to the oscillation of the radial bed slope, the values of the individual terms in the momentum equation also oscillate along the bend. The principal opposing terms are the gravity and bed-shear forces, terms 4 and 6. Examination of (23) for this and several other flows revealed that term 3 is much smaller than term 1 except for flows in bends with very sharp channel curvature. Therefore, term 3 is not included in Figs. 9 and 10. Because run T1 is a mild-bend flow, the magnitudes of terms 1 and 2 are smaller than terms 4 and 6, but the former have larger amplitudes of

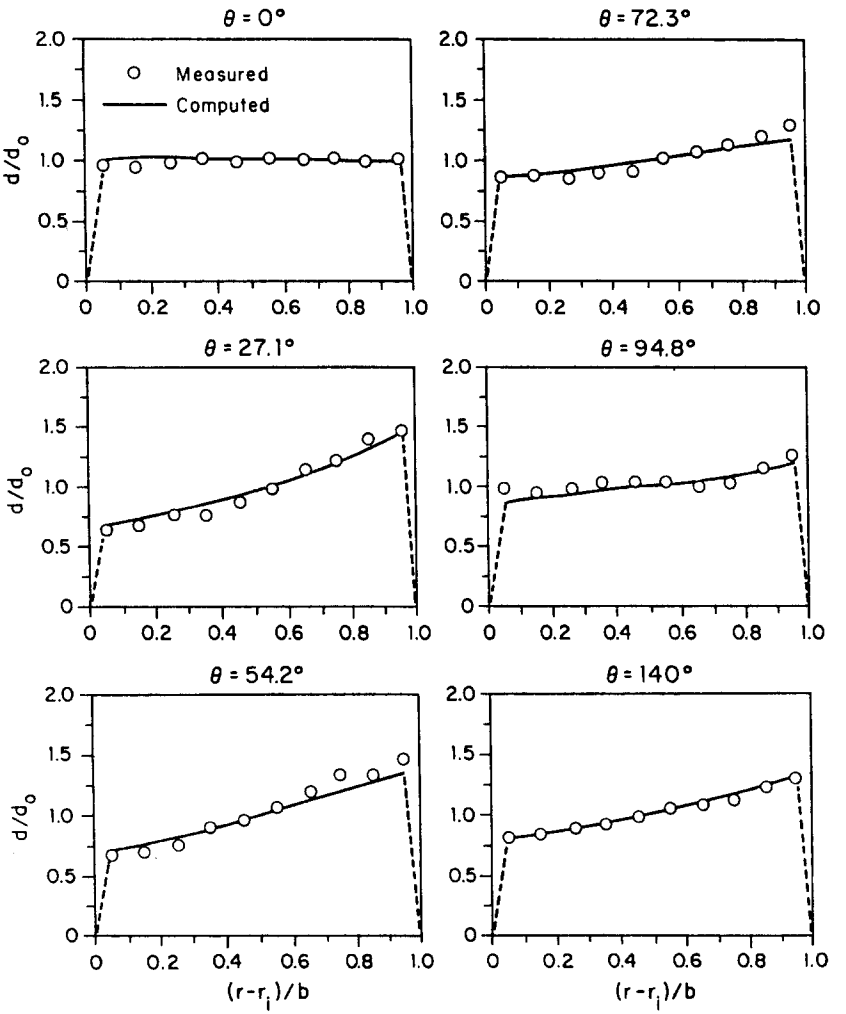

FIG. 7. Measured and Computed Lateral Distributions of d/d_0 at Representative Sections for Struiksma's (1983) Run T1

oscillation than the latter. For comparison, Fig. 10 shows the magnitudes of the terms (except term 3) in (23) for Kikuchi et al.'s (1988) run 1 [Table 1 in Yeh and Kennedy (1993)]. It can be seen that terms 1 and 2 undergo opposing swings near the ends of the curve, but elsewhere all terms are nearly constant. These two terms each demonstrate minor extrema following their first major ones, but these oscillations are very small compared to those of the erodible-bed flow (Fig. 9).

Sensitivity analyses of $\bar{S}_T$ to η and C_b (Yeh 1990) revealed that the computed results are fairly sensitive to both.

The third of Struiksma's (1983) experiments, run T3, was computed using the parameter values given previously. The computed results again were found to be satisfactory. Comparisons of the computed streamwise varia-

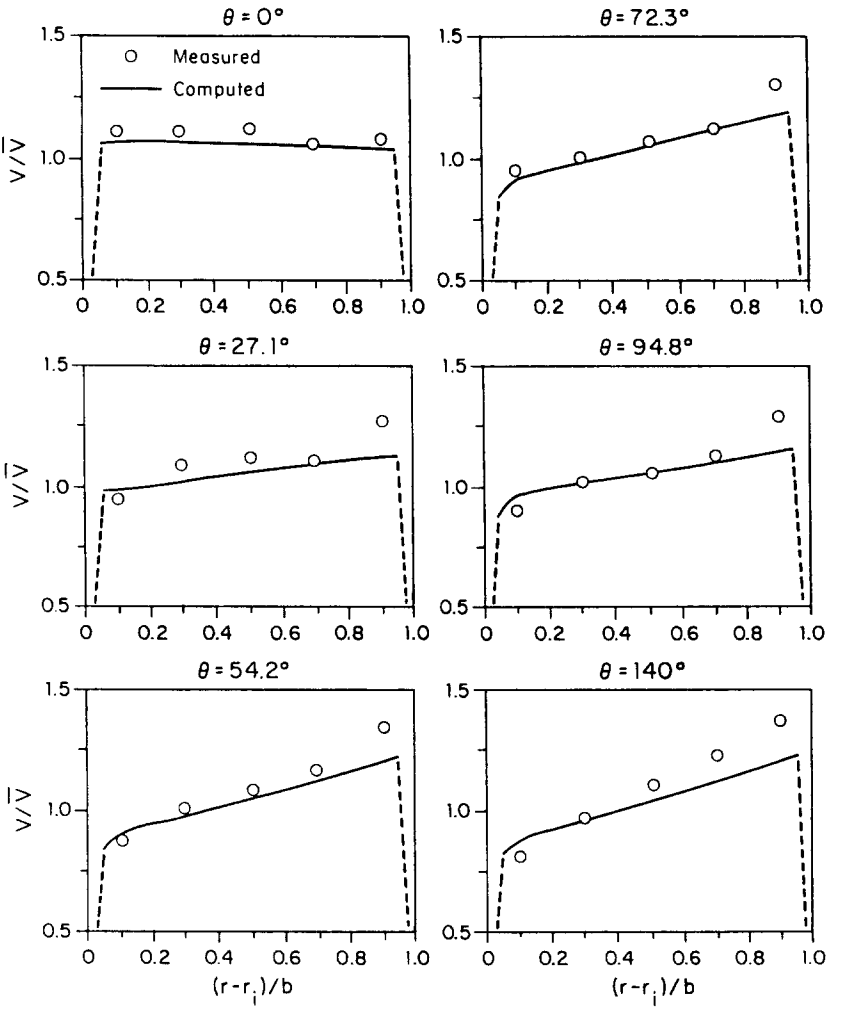

FIG. 8. Measured and Computed Lateral Distributions of $V/\bar{V}$ at Representative Sections for Struiksma's (1983) Run T1

tions of d/d_0 along lines at $0.25b$ and $0.75b$ from the inside wall for Struiksma's (1983) three runs with computed results obtained from other investigators' models are shown in Fig. 11. Note that the computed results reported by Struiksma et al. (1985) utilized different values of the model parameters for runs T1 and T2 than for run T3.

The model was also evaluated with two other experiments: Odgaard and Bergs' (1988), and Olesen's (1985) run T5, both summarized in Table 1. Instead of using the centerline-average value of depth ($d_0 = 0.15$ m) given by Odgaard and Bergs (1988), the cross-sectional average depth, $d_0 = 0.165$ m, was adopted for their run. The friction factor then changes slightly, from their reported value of 0.067–0.074. Fig. 12 shows the streamwise variations of d/d_0 near the walls. It can be seen that the computed oversteepening of

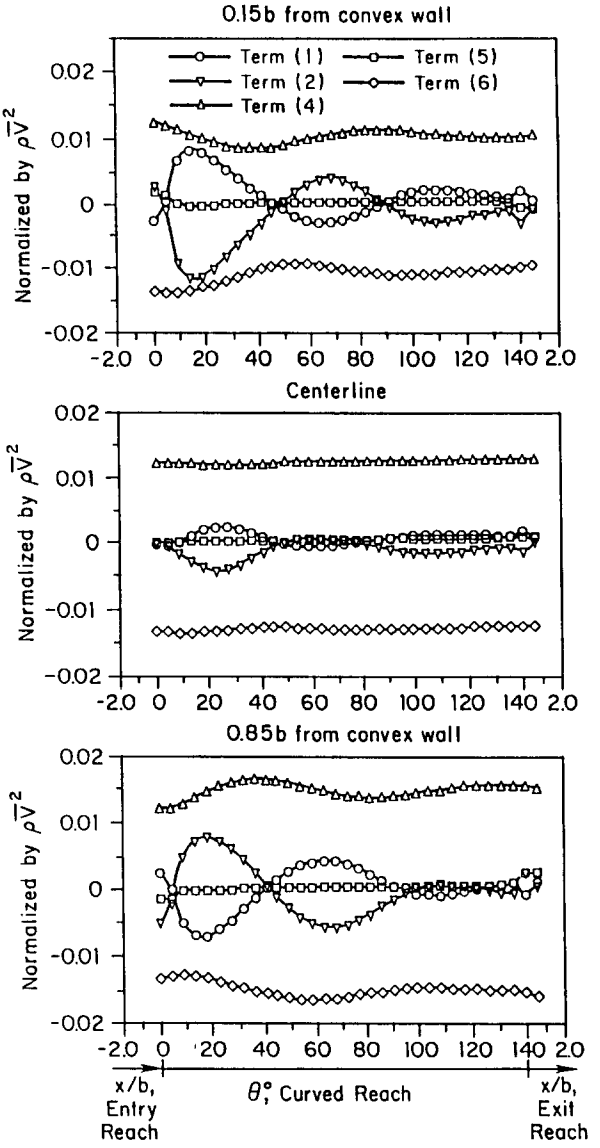

FIG. 9. Computed Streamwise Variations of Lettered Terms in Momentum Equation [(23)] for Struiksma's (1983) Run T1 (Note: Term 3 ≈ 0)

the bed has almost no oscillation after the initial overshoot (i.e., $\bar{S}_T$ is "overdamped," in some sense, for this flow), which is different from the result computed by Odgaard and Bergs (1988). Olesen's experiments differ from Struiksma's (1983) mainly in the distribution of grain sizes (see Table 1). Olesen (1985) pointed out that the measured bed topography seems to indicate that the gradation of the bed material has only a modest influence on the bed configuration provided that the sediment enters the bend uni-

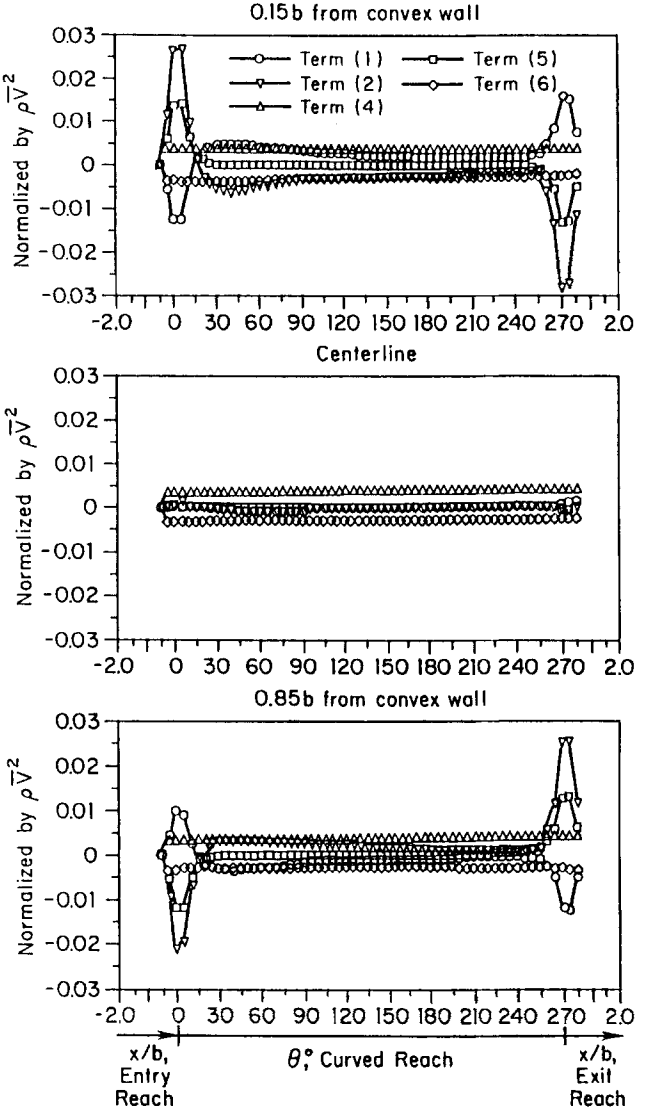

FIG. 10. Computed Streamwise Variations of Lettered Terms in Momentum Equation [(23)] for Kikuchi et al.'s (1988) Run 1 (Note: Term 3 ≃ 0)

formly distributed across the channel. Therefore, only run T5 of his investigation was computed in the present study. When the values of the parameters related to sediment transport, $\eta = 0.2$ and $C_b = 0.75$, determined from Struiksma's (1983) runs T1 and T2 were used, the computed radial oversteepening of the bed was found to be somewhat smaller than measured. (Note that D_{50} in run T5 was almost twice as large as that in runs T1–T3.) This suggests that the parameters η and C_b in (13) and (15), respectively, are dependent on the bed-particle size. It may be that the interactions among

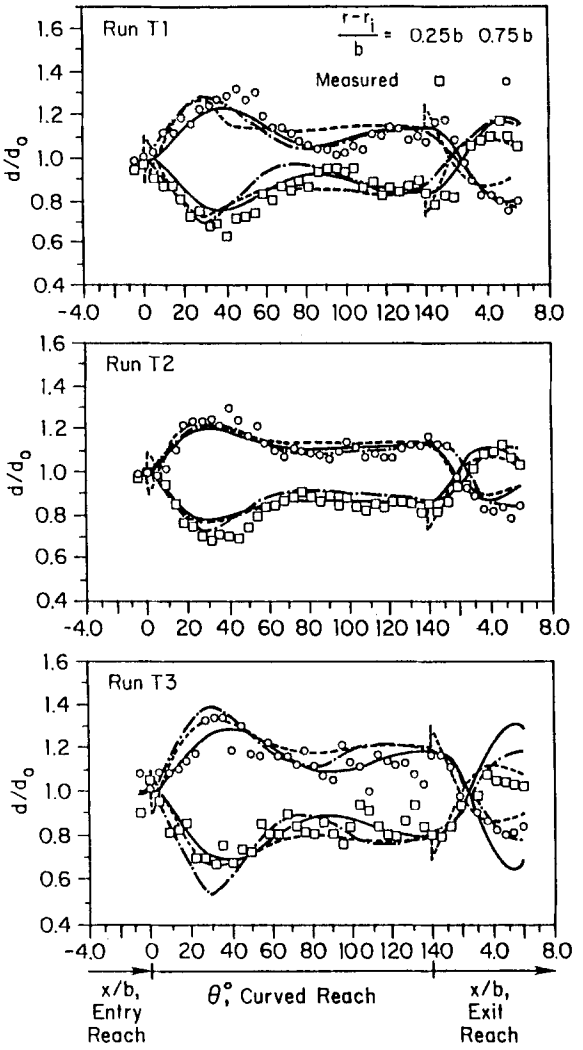

FIG. 11. d/d_0 **at 0.25**b **and 0.75**b **from Convex Wall Measured by Struiksma (1983); and Computed by Present Model (——), Struiksma et al. (1985) (—·—·—), and Johannesson (1988) (----)**

the flow, bed topography, and two-dimensional sediment discharge are so complex that simplified relations such as (13) and (15) cannot be applied universally without modification. By adopting $\eta = 0.15$ and $C_b = 0.45$, the computed streamwise variation of d/d_0 near the walls presented in Fig. 13 was obtained. Generally speaking, the overall computed results are satisfactory if the modified values of η and C_b are adopted. The computed results using the calibrated values ($\eta = 0.2$ and $C_b = 0.75$) are also plotted in Fig. 13 for comparison.

The present formulation is basically applicable to flows with moderately and highly nonuniform bed sediments. If other representative particle size

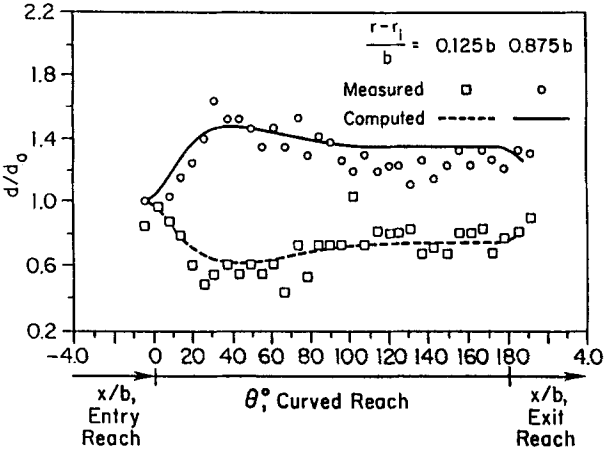

FIG. 12. Measured and Computed d/d_0 at $0.125b$ and $0.875b$ from Convex Wall for Odgaard and Bergs' (1988) Experiment

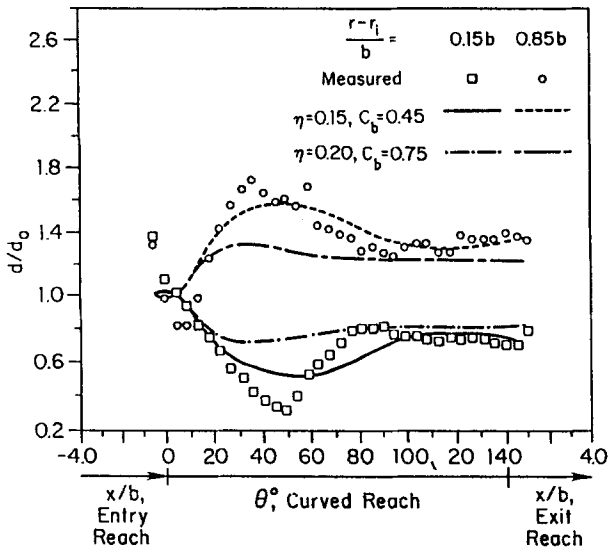

FIG. 13. Measured and Computed d/d_0 at $0.15b$ and $0.85b$ from Convex Wall for Olesen's (1985) Run T5

instead of D_{50} is used, parameters η and C_b, which are included in the sediment transport model, need to be calibrated again.

Conclusions

The hybrid integral-differential moment and momentum formulation of rigid-boundary channel flow was extended to the case of erodible-bed flows to obtain a set of equations which describe the flow field, bed topography, and 2D sediment discharge in erodible-bed channel bends. The formulations

for the fixed- and erodible-bed cases differ principally in that the 2D sediment-continuity relations and streamwise (θ) and radial (r) sediment-transport relations are incorporated into the latter to calculate the variable bed elevation or flow depth, $d(r, \theta)$, in the bend. A power-law relation relating the streamwise unit sediment discharge to a power of the local mean velocity was adopted. The radial unit sediment discharge was formulated under the assumption that the ratio of radial to streamwise unit sediment discharges is proportional to the ratio of the excess (above that required to balance the radial bed shear stress) radial component along the bed of the submerged weight of the sediment bed-layer to the streamwise bed shear stress. The model contains six parameters: ξ, γ, α, and β [(16), (17), (20), and (21) in part I); and η and C_b [(13) and (15), for erodible-bed flows only]. The best estimates of the first four are $\xi = 0.5$, $\gamma = 0.3$, $\alpha = 6$, and $\beta = 1$, obtained from calibration of the fixed-bed model (part I). The best estimates of the last two values are $\eta = 0.2$ and $C_b = 0.75$.

The principal conclusions may be summarized as follows.

The flow field and bed topography along a bend, including the reaches of transition flow (produced by changes in channel curvature) and fully developed flow, are well predicted by the model.

The r and θ distributions of V and the position and magnitude of the overshoot and subsequent spatial damped oscillatory behavior of the average radial bed slope, $\bar{S}_T$, are accurately described by the model, as are other features of the bed topography. Due to the oscillation of $\bar{S}_T$, both $\bar{U}$ and $\bar{U}_t$ (the average secondary rotational and translational velocities) also exhibit oscillatory behavior along the bend. This oscillatory behavior is neither predicted nor observed for the fixed-bed case.

A simple relation, (13), based on physical reasoning and concepts related to unidirectional sediment transport, between the lateral sediment discharge and the radial nonequilibrium bed slope appears to work quite well. It may, however, need further refinement to adequately account for effects of bed-sediment size.

Due to the deformation of the channel bed, the shift of maximum primary-flow velocity toward the outer wall region occurs upstream of that in the fixed-bed case, and the distortion of the radial depth-averaged-velocity profile is more pronounced.

As in the fixed-boundary case, the relative magnitudes of terms in the θ momentum equation depend on the sharpness of the channel curvature. The conclusions concerning their relative magnitudes reached for the fixed-bed case apply also to erodible-bed bends, except for some effects due to the oscillatory behavior in the latter case. Due to the oscillation of the radial bed slope, all terms in the θ momentum equation have corresponding oscillatory behavior, with the terms $\partial(uv)/\partial r$ and $1/r\,\partial v^2/\partial\theta$ exhibiting the largest oscillations.

ACKNOWLEDGMENTS

The writers gratefully acknowledge support of this work by the Iowa investor-owned electric utilities through the University of Iowa's Institute of Hydraulic Research, under its EPRIa program. Particular thanks are due to Syunsuke Ikeda, Visiting Professor at IIHR from the Tokyo Institute of Technology in 1988, for his keen insight and invaluable suggestions during key phases of development of the mathematical model.

APPENDIX I. REFERENCES

Falcon, M. A., and Kennedy, J. F. (1983). "Flow in alluvial-river curves." *J. Fluid Mech.*, 133, 1–16.

Ikeda, S., and Nishimura, T. (1986). "Flow and bed profile in meandering sand-silt rivers." *J. Hydr. Engrg.*, ASCE, 112(7), 562–579.

Karim, F., and Kennedy, J. F. (1981). "Computer-based predictors for sediment discharges and friction factors of alluvial streams." *IIHR Report No. 242*, Univ. of Iowa, Iowa City, Iowa.

Kikuchi, M., Ikeda, S., and Yamasaka, M. (1988). "A basic study on the three-dimensional flow in a bend." *Proc., 43rd Conf.*, Japan Society of Civil Engineers, Tokyo, Japan, 109–110.

Nelson, J. M. (1988). "Mechanics of flow and sediment transport over nonuniform erodible bed," PhD thesis, Univ. of Washington, Seattle, Washington.

Odgaard, A. J. (1986). "Meander flow model. I: Development." *J. Hydr. Engrg.*, ASCE, 112(12), 1117–1136.

Odgaard, A. J., and Bergs, M. A. (1988). "Flow processes in a curved alluvial channel." *Water Resour. Res.*, 24(1), 45–56.

Olesen, K. W. (1985). "Experiments with graded sediment in the DHL curved flume." *Rep. on Experimental Investigation R657-XXII M1771*, Delft Univ. of Technology, Delft, The Netherlands.

Parker, G., and Johannesson, H. (1989). "Observations on several recent theories of resonance and overdeepening in meandering channels." *River meandering*, S. Ikeda and G. Parker, eds., American Geophysical Union (AGU), Washington, D.C., 379–415.

Shimizu, Y., Yamaguchi, H., and Itakura, T. (1990). "Three-dimensional computation of flow and bed deformation." *J. Hydr. Engrg.*, ASCE, 116(9), 1909–1108.

Simons, D. B., and Sentürk, F. (1977). *Sediment transport technology*. Water Resources Publications, Fort Collins, Colo.

Struiksma, N. (1983). "Results of movable bed experiments in the DHL curved flume." *Rep. on Experimental Investigation R657-XXIII M1771*, Delft Univ. of Technology, Delft, The Netherlands.

Struiksma, N., Olesen, K. W., Flokstra, C., and de Vriend, H. J. (1985). "Bed deformations in curved alluvial channels." *J. Hydr. Res.*, 23(1), 57–79.

Yeh, K. C. (1990). "Flow and bed topography in fixed-channel and river bends," PhD thesis, University of Iowa, Iowa City, Iowa.

Yeh, K. C., and Kennedy, J. F. (1993). "Moment model of nonuniform channel-bend flow. I: Fixed beds." *J. Hydr. Engrg.*, ASCE, 119(7), 776–795.

APPENDIX II. NOTATION

The following symbols are used in this paper:

b = channel width;
C_b = correction factor in (15);
D_{50} = median sediment-particle size;
d, d_0 = flow depth; subscript 0 signifies upstream uniform-flow depth;
d_{in}, d_{ou} = flow depths at inner and outer walls;
F = constant defined by (11);
f = Darcy-Weisbach friction factor;
g = acceleration of gravity;
G, H, I, J = constants in (4) and (5), defined by (6)–(9);
K = exponent in sediment-transport relation in (18);
M_r, M_θ = r and θ components of MOM;
$n(\theta)$ = inverse exponent in power-law velocity profile;
p_s = bed-material porosity;

q_r, q_θ = radial and streamwise unit sediment discharges;
$\bar{q}_\theta$ = value of q_θ corresponding to $\bar{V}$;
r = radial coordinate, or channel streamline radius;
r_i, r_o, r_c = radii of inner, outer, and centerline channel radii;
S_0 = streamwise bed slope;
$S_T(r, \theta)$ = local radial bed slope;
S_{T0} = equilibrium radial bed slope;
$\bar{S}_T(\theta)$ = average radial bed slope;
$\bar{S}_T$ = $\bar{S}_T b/(2d_0)$ = normalized average radial bed slope;
$U(r, \theta)$ = surface value of secondary rotational velocity, u_s;
$\bar{U}(\theta)$ = section-averaged U;
$\bar{U}_t(\theta)$ = cross-sectional-averaged u_t;
u, v, w = velocity components in the r, θ, z directions;
$u_s(r, \theta, z)$ = secondary rotational velocity;
$u_t(r, \theta)$ = secondary translational velocity;
u_* = shear velocity;
u_{*c} = critical shear velocity for the initiation of bed-material motion;
$V(r, \theta)$ = depth-averaged v;
y_b = bed-layer thickness;
z_b, z_w = bed and water surface elevations;
α, β = constants in (20) and (21) in part I and (3) and (4) in part II;
γ = constant in (17) in part I;
δ = correction factor in (1);
η = constant in (13);
θ_0 = bend included angle;
ρ, ρ_s = densities of fluid and sediment particles;
ρ' = $\rho_s - \rho$;
τ_{0j} = boundary shear stress;
φ = dimensionless shear stress obtained from Shields' diagram; and
ω = relaxation parameter in (21).